JACC: CARDIOVASCULAR IMAGING VOL. 1, NO. 3, 2008

ISSN 1936-878X/08/$34.00
PUBLISHED BY ELSEVIER INC. DOI:10.1016/j.jcmg.2008.01.014

Correspondence Between the 17-Segment Model and Coronary Arterial Anatomy Using Contrast-Enhanced Cardiac Magnetic Resonance Imaging

José T. Ortiz-Pérez, MD, José Rodríguez, MD, Sheridan N. Meyers, MD, FACC, Daniel C. Lee, MD, Charles Davidson, MD, FACC, Edwin Wu, MD
Chicago, Illinois

OBJECTIVES The purpose of this study was to investigate the correspondence between the coronary arterial anatomy and supplied myocardium based on the proposed American Heart Association 17-segment model.

BACKGROUND Standardized assignment of coronary arteries to specific myocardial segments is currently based on empirical assumptions.

METHODS A cardiac magnetic resonance study was performed in 93 subjects following acute myocardial infarction treated with primary percutaneous coronary intervention. Two observers blindly reviewed all angiograms to examine the location of the culprit lesion and coronary dominancy. Two additional observers scored for the presence of cardiac magnetic resonance hyperenhancement (HE) on a 17-segment model. Segments were divided based on anatomical landmarks such as the interventricular grooves and papillary muscles.

RESULTS In a per-segment analysis, 23% of HE segments were discordant with the empirically assigned coronary distribution. Presence of HE in the basal anteroseptal, mid-anterior, mid-anteroseptal, or apical anterior wall was 100% specific for left anterior descending artery occlusion. The left anterior descending artery infarcts frequently involved the mid-anterolateral, apical lateral, and apical inferior walls. No segment was 100% specific for right coronary artery or left circumflex artery (LCX) occlusion, although HE in the basal anterolateral wall was highly specific (98%) for LCX occlusion. Combination of HE in the anterolateral and inferolateral walls was 100% specific for a LCX occlusion, and when extended to the inferior wall, was also 100% specific for a dominant or codominant LCX occlusion.

CONCLUSIONS Four segments were completely specific for left anterior descending artery occlusion. No segment can be exclusively attributed to the right coronary artery or LCX occlusion. However, analysis of adjacent segments increased the specificity for a given coronary occlusion. These findings bring objective evidence in the appropriate segmentation of coronary arterial perfusion territories and assist accurate assignment of the culprit vessel in various imaging modalities. (J Am Coll Cardiol Img 2008;1:282–93) © 2008 by the American College of Cardiology Foundation

From the Feinberg Cardiovascular Research Institute and Division of Cardiology, Northwestern University Feinberg School of Medicine, and the Bluhm Cardiovascular Institute, Northwestern Memorial Hospital, Chicago, Illinois. Dr. Wu received grants from the GlaxoSmithKline Research and Education Foundation for Cardiovascular Disease, the American Heart Association Scientist Development Grant, and the Feinberg Cardiovascular Research Institute and Department of Medicine. Drs. Ortiz-Pérez and Rodríguez were supported by grants from the Spanish Society of Cardiology.

Manuscript received October 5, 2007; revised manuscript received December 13, 2007, accepted January 3, 2008.

To make appropriate clinical decisions concerning diagnosis and treatment, integration of information between noninvasive functional imaging techniques and invasive coronary angiography is essential. The American Heart Association (AHA) Writing Group on Myocardial Segmentation and Registration for Cardiac Imaging recommends a 17-segment model of the left ventricle as an optimally weighted approach for the visual interpretation of regional left ventricular (LV) abnormalities by multiple cardiac imaging techniques (1). Individual myocardial segments were assigned to coronary artery territories based on available data with little correlation with delineated myocardial segmentation (2). Cardiac magnetic resonance (CMR) imaging has emerged as a powerful noninvasive technique for the evaluation of myocardial function, perfusion, and viability in a single study without the need of radioactive tracers administration, which is a distinct attribute of CMR (3,4). This imaging modality has been shown to have a higher spatial resolution when compared to nuclear perfusion imaging techniques (5). Additionally, specific structures of the left ventricle, such as the right ventricular insertion points and papillary muscles, can be readily identified to register segments from one modality to another.

We have previously demonstrated that the subendocardial extent of hyperenhancement (HE) following ST-segment elevation myocardial infarction (STEMI) closely matches the myocardial bed at risk determined by angiography (6). The purpose of this study was to assess the correspondence between the coronary arteries distribution by invasive angiography and their supplied myocardium according to the 17-segment model by using contrast-enhanced CMR imaging in a cohort of patients with first STEMI presenting for primary percutaneous coronary intervention (PCI).

METHODS

From a prospective study that investigated LV remodeling following STEMI carried out between January 2000 and June 2006, we retrospectively identified 115 subjects who met the following criteria: 1) presence of chest pain for at least 30 min with electrocardiographic ST-segment elevation $\geq$0.1 mV in at least 2 adjacent leads or suspicion of true posterior infarction; 2) attempted primary PCI during the first 24 h of admission; 3) confirmation of acute myocardial infarction by creatine phosphokinase release above twice the upper limit of normal; and 4) absence of clinical history or electrocardiographic evidence of prior myocardial infarction, hemodynamic instability precluding the CMR study, or other formal contraindication for CMR imaging. We excluded 11 subjects with initial Thrombolysis In Myocardial Infarction (TIMI) flow grade >1 in the infarct-related artery (IRA), 2 subjects with previous coronary bypass surgery, and 1 subject with uncertain identification of the IRA. A total of 101 eligible subjects had their CMR images reviewed for this study. All subjects signed consent forms for their participation in the study, which was approved by the Northwestern University Institutional Review Board.

Coronary angiography. Selective coronary angiography was performed with a biplane system and a standard femoral approach. All studies were reviewed by consensus of 2 experienced angiographers who were masked to the CMR data. The identification of the culprit lesion in the IRA was easily made in all cases based on the angiographic characteristics, the distal TIMI blood flow, the electrocardiographic findings, and the response to treatment. The site of the culprit lesion occlusion, as well as the severity and location of other significant lesions were visually assessed and registered according to classical landmarks. A proximal left anterior descending (LAD) artery occlusion was considered when the site of occlusion occurred proximally to the first septal or diagonal branch and a mid-LAD occlusion from the first septal or diagonal branch to the next diagonal branch. Proximal left circumflex (LCX) occlusions were considered those located previous to the first relevant marginal branch, and mid-LCX was any occlusion between the first marginal and the second marginal or posterolateral branch. All right coronary artery (RCA) occlusions were located before the takeoff of the posterior descending artery. The coronary tree was considered right dominant when the posterior descending artery and posterolateral branches originated from the RCA and left dominant when they both originated from the LCX. A balanced coronary circulation was defined when the PDA originated from the RCA and all posterolateral branches from the LCX. All subjects received aspirin and heparin, and most were also treated with glycoprotein IIb/IIIa inhibitors and clopidogrel. With the exception of 1 subject with a failed revascu-

ABBREVIATIONS AND ACRONYMS

AHA = American Heart Association
CMR = cardiac magnetic resonance
HE = hyperenhancement
IRA = infarct-related artery
LAD = left anterior descending
LCX = left circumflex
LV = left ventricular
PCI = percutaneous coronary intervention
RCA = right coronary artery
STEMI = ST-segment elevation myocardial infarction
TIMI = Thrombolysis In Myocardial Infarction

larization procedure, all patients received at least 1 stent in the culprit lesion.

CMR. All studies were performed at a mean of 2.9 ± 2 (range 1 to 7 days) after the admission. A total of 70 patients returned for a second CMR study at a mean of 5 ± 3.1 months later. Subjects were imaged in supine position in a 1.5-T Sonata or Avanto scanner (Siemens, Erlangen, Germany) and imaged with a dedicated cardiac phased-array receiver coil. Standard steady state free precession cines were taken during breath-holds in the 3 long axis views and contiguous 6-mm short axis slices every 10 mm from the mitral annulus to the LV apex. Ten to 15 min following intravenous gadolinium at a dose of 0.2 mmol/kg, delayed contrast-enhanced images were acquired in identical slice positions using a inversion-recovery segmented gradient-echo sequence (7). Inversion times were adjusted to null normal myocardium (230 to 350 ms). Typical imaging parameters were as follows: field of view 360 to 400 mm, matrix size 256, echo time 4 ms, repetition time 40 ms, typical voxel size 1.4 × 1.4 × 6 mm.

Data analysis. All images were de-identified for the analysis. Representative basal, mid-ventricular, and apical slices as well as the 2-chamber long axis views were visually evaluated by a consensus of 2 experienced observers to determine the presence or absence of HE, defined as areas with a mean signal intensity more than 2 standard deviations above that of normal myocardium, in each 1 of the 17 LV segments. Segments were divided as previously proposed (1). Division between the anterior and anteroseptal segments was made at the anterior interventricular groove and extended posteriorly through the center of the left ventricle to divide the inferior and inferolateral segments. Likewise, the inferoseptal and inferior segments and the anterior and anterolateral segments were divided by the posterior interventricular groove. The anteroseptal and inferoseptal as well as the anterolateral and inferolateral segments were divided halfway between the anterior and inferior interventricular grooves. In the apical segments, the anteroseptal and inferoseptal segments were combined to form the apical septum segment and the anterolateral and inferolateral segments were combined to form the apical lateral segment.

A segment was considered affected if HE was present in more than 50% of the circumferential extent for that segment, and segments with any wall motion abnormality were additionally noted. Adjacent short axis views to the representative basal, mid, or apical views were used to confirm or reject the location and presence of any HE. Additionally, the endocardium and epicardium was planimetered in sequential short axis contrast-enhanced images, and the circumferential extent of the infarct was computed as the percentage of the endocardial surface presenting HE. Ejection fraction, indexed LV volumes, and infarct size—expressed as percentage of LV wall volume—were computed as previously described (6).

The specificity and predictive accuracy of the presence of HE in each segment of the 17-segment model for the diagnosis of LAD, RCA, or LCX occlusion was calculated irrespective of the location—proximal, mid, or distal—of the culprit lesion. Quantitative variables are expressed as mean ± standard deviation. One-way analysis of variance was used to compare the infarct circumferential extent and CMR-derived parameters between groups, and Kruskal-Wallis test was performed to compare the mean number of segments with HE according to the IRA. Chi-square test was applied for comparison of qualitative variables between groups. Paired t test was used to compare the number of segments with HE at baseline and follow-up and the number of segments with wall dysfunction. A p value < 0.05 was considered statistically significant.

RESULTS

Of the 101 available subjects, 93 had a single isolated area of HE. None had an additional coronary occlusion other than the IRA, although 20 of them were treated with an additional PCI of a significant nonculprit lesion before the CMR study. Table 1 depicts clinical and angiographic characteristics of the study population. There were no differences in risk factors profile, multivessel disease, time-to-reperfusion, final TIMI flow grade, and collateral grades according to the IRA. Figure 1 demonstrates representative division of the contrast-enhanced CMR studies into 17 segments following STEMI to the LAD, RCA, and LCX arteries.

The remaining 8 subjects had 2 separate areas of HE clearly isolated and surrounded by normal myocardium and were excluded from the analysis. Seven of them had a severe lesions—6 cases with a chronic total or subtotal occlusion and 1 case with a 70% stenosis—in a vessel different than the IRA that could explain the presence of these additional areas of HE. For each of these cases, a representative single slice with its corresponding finding in the

Table 1. Clinical and Angiographic Characteristics of the Study Population

	Total (n = 93)	Culprit Artery		
		LAD (n = 44)	RCA (n = 34)	LCX (n = 15)
Clinical data				
Age (yrs)	57 ± 11	58 ± 11	59 ± 10	53 ± 10
Male (%)	84	84	82	87
Diabetes (%)	15	11	18	20
Dyslipidemia (%)	54	52	48	67
Hypertension (%)	51	43	54	67
Smoker (%)	49	41	58	60
Multivessel disease (%)	59	50	79	40
Right dominance (%)	78	71	94	67
Final TIMI flow 3 (%)	90	89	91	93
Time-to-reperfusion (min)*	199 [135 to 345]	210 [148 to 390]	160 [104 to 283]	210 [165 to 450]
Good collaterals (%)	42	39	56	27
CMR data				
Ejection fraction (%)	41.5 ± 9.6	35.8 ± 9.5	47.4 ± 5.3	44.6 ± 13.4
End-diastolic volume index (ml/m^2)	78.1 ± 16.0	79.0 ± 17	75.4 ± 15.5	82.1 ± 14.3
End-systolic volume index (ml/m^2)	45.6 ± 14.5	50.0 ± 16	39.9 ± 10.2	46.1 ± 13.4
Infarct size (% LV wall volume)	21.6 ± 11.2	28.1 ± 11.5	15.1 ± 6.4	17.8 ± 6.0

Data expressed as percentage or mean ± standard deviation. *Data represents median [25th to 75th percentiles].
CMR = cardiac magnetic resonance; LAD = left anterior descending; LCX = left circumflex; LV = left ventricular; RCA = right coronary artery; TIMI = Thrombolysis In Myocardial Infarction.

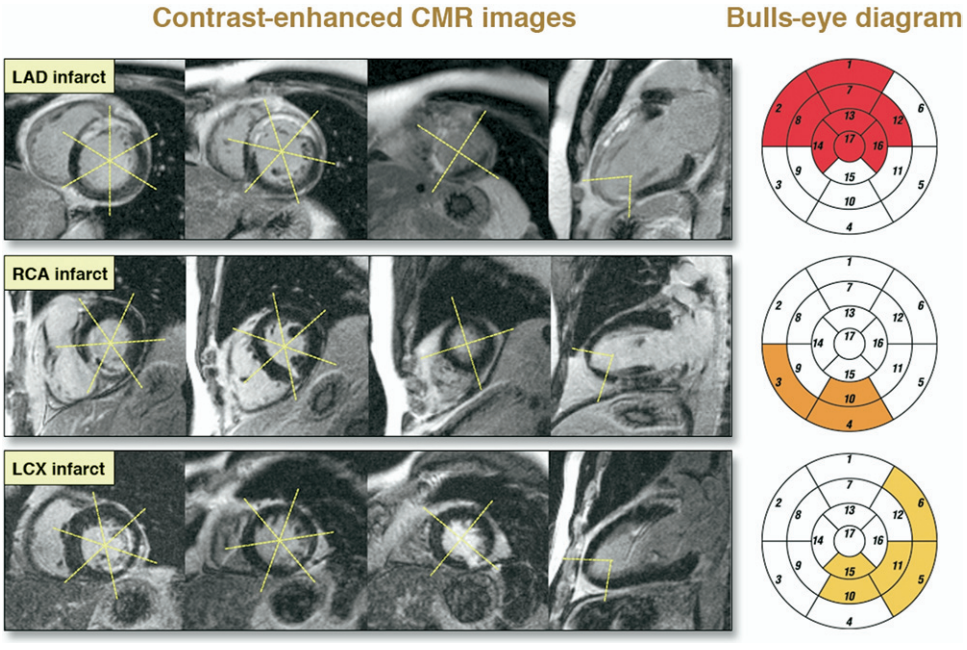

Figure 1. Representative Segmentation and Pattern of Contrast HE Over 17-Segments of the LAD, RCA, and LCX Arteries

A single basal, mid, apical, and 2-chamber contrast-enhanced views of 3 subjects **(left panels)** following an acute myocardial infarction with occlusion to the left anterior descending (LAD) artery, right coronary artery (RCA), and left circumflex (LCX) artery. The **dotted yellow lines** delineate and separate the 17-segments over the entire left ventricle. Bulls-eye diagrams **(right)** reveal the pattern of infarction for each example. CMR = cardiac magnetic resonance; HE = hyperenhancement.

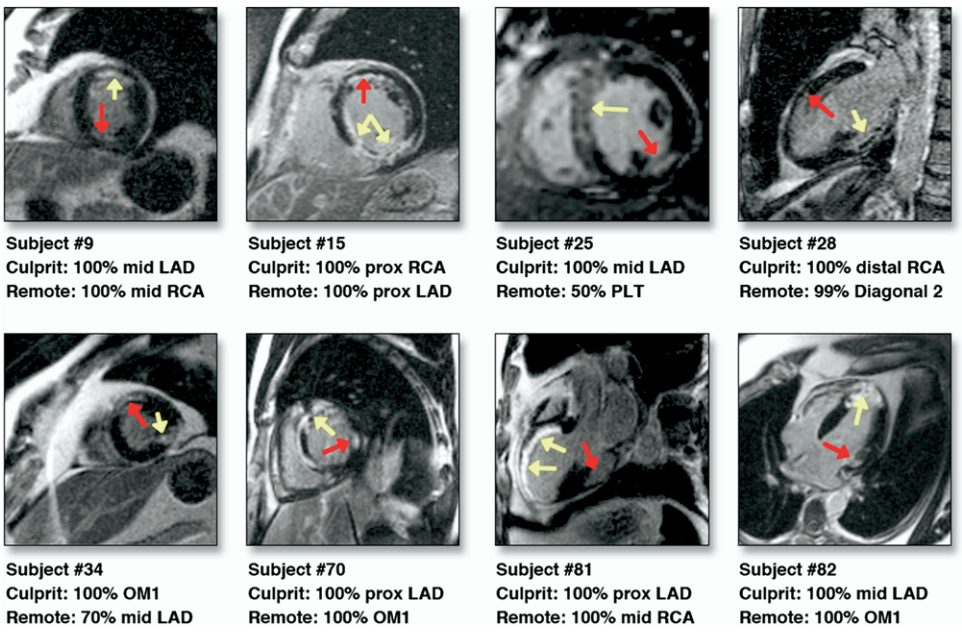

Figure 2. Patients With Unrecognized Previous Myocardial Infarction

A single representative delayed enhanced image with the corresponding findings in the catheterization lab for each of the 8 subjects is presented. The **yellow arrows** point out the acute infarct, and the **red arrows** point to the remote infarct. OM1 = obtuse marginal artery; PLT = platelet; other abbreviations as in Figure 1.

cardiac catheterization laboratory is presented in Figure 2.

Subjects with LAD occlusion showed lower ejection fractions and greater infarct sizes than subjects with either LCX or RCA occlusion ($p < 0.01$ for all). They also had higher number of segments with HE (7.7 ± 2.1) than subjects with LCX (5.1 ± 2.4) or RCA occlusion (4.3 ± 1.5) ($p < 0.001$ for both). The infarct circumferential extent was also higher in patients with LAD than LCX or RCA occlusion, 40.1 ± 10.0, 26.9 ± 7.3, and 23.1 ± 5.8, respectively ($p < 0.001$ for both). No significant difference was observed in the number of segments with HE and circumferential extent between the RCA and LCX occlusion, $p = 0.6$ and $p = 0.5$, respectively.

HE distribution according to the IRA. A bulls-eye representation with specificities of HE distribution according to the culprit artery is presented in Figure 3A. At baseline, the presence of HE in the basal anteroseptal (segment 2), mid-anterior (segment 7), mid-anteroseptal (segment 8), or apical anterior segment (segment 13) was 100% specific for LAD occlusion. In subjects with anterior infarction, involvement of the basal anteroseptum (segment 2) was, in addition, highly specific (85%) for proximal LAD occlusion. No individual segment was 100% specific for RCA or LCX occlusion. However, among 9 studies with HE in the basal anterolateral wall (segment 6), 7 had an occlusion in the LCX, 1 in the LAD, and another in a ramus. Thus, involvement of this segment was highly specific (98%) for LCX occlusion. The basal inferolateral wall (segment 5) was also highly specific (95%) for LCX occlusion. The basal inferior wall (segment 4) was the most specific (93%) for RCA occlusion, although this segment was additionally involved in 4 cases of dominant or codominant LCX occlusion. The positive predictive value of the presence of HE in every segment for each coronary artery is shown in Table 2.

An additional analysis, taking into account adjacent segments, was performed to distinguish between RCA and LCX occlusions. Thus, any combination of HE in the inferolateral wall (segments 5 or 11) with HE in the anterolateral wall (segments 6 or 12) was 100% specific for an occlusion of the LCX or ramus. Furthermore, the presence of any HE in the anterolateral wall in combination with any HE in the inferior wall (segments 4 or 10) was 100% specific for dominant or codominant LCX occlusion. Figure 4 illustrates 3 examples of LCX occlusion with variable extent of HE depending on the dominance and the site of the occlusion.

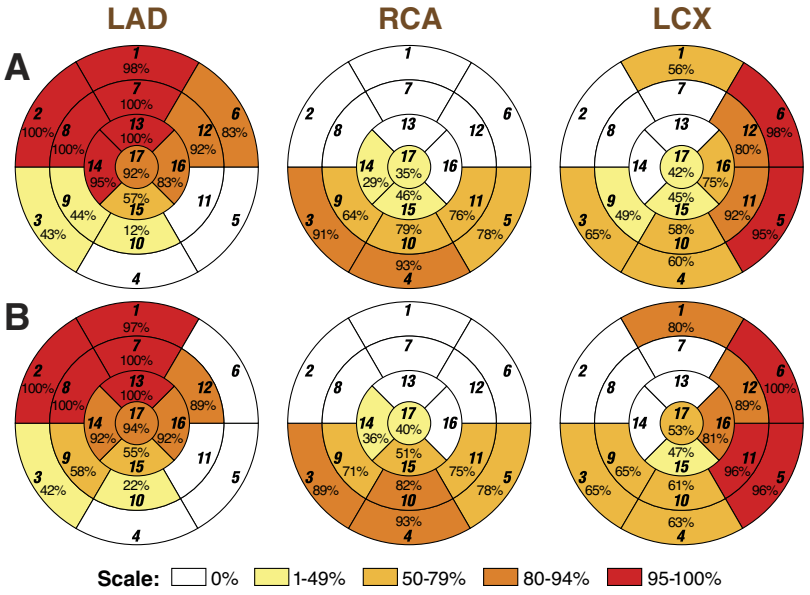

Figure 3. Specificity of Segmental HE According to the IRA Acutely and on Follow-Up

Bulls-eye diagrams showing the distribution and specificities of CMR HE according to the infarct related artery (IRA). At baseline, only 4 segments were 100% specific for LAD occlusion and none for RCA or LCX occlusion **(A)**. At follow-up, the basal anterolateral segment was 100% specific for LCX occlusion **(B)**. No major changes were seen in the HE distribution between baseline and follow-up studies. **Italicized numbers** designate the segment number. Abbreviations as in Figure 1.

The greatest variability in coronary distribution occurred at the inferoapical wall (segment 15), with specificities of 57%, 45%, and 46% for occlusion of the LAD, LCX, and RCA, respectively.

Change in ce-CMR distribution. Infarcted myocardium decreased from 20.3 ± 10.3% to 16.2 ± 10.5%; $p < 0.001$, which represents a relative 21.5 ± 3.7% reduction in the mean initial infarct size. The number of segments with any HE decreased from 6.0 ± 2.5 to 5.3 ± 2.6; $p < 0.001$. Figure 3B is an additional diagram with specificities of HE distribution at follow-up. There were no major changes in HE distribution between baseline and follow-up studies. According to infarct location, infarct size significantly decreased among patients with LAD infarction (n = 34, from 26.1 ± 9.8% to 20.5 ± 11.0%; $p < 0.001$) and non-LAD infarction (n = 36, from 15.4 ± 7.6% to 12.6 ± 8.4%; $p = 0.001$). Similarly, the number of segments with any HE decreased among patients with LAD (7.5 ± 2.1 vs. 6.7 ± 2.6, $p < 0.01$) and non-LAD infarctions as well (4.7 ± 2.0 vs. 4.2 ± 2.0, $p = 0.001$).

Segmental wall motion according to the IRA. Figure 5 depicts the specificities of segmental wall motion abnormalities according to the IRA. In a per-patient analysis, the number of segments with HE was not different from the number of segments with wall motion abnormalities (6.0 ± 2.6 vs. 6.3 ± 3.3, respectively, $p = 0.3$). However, in a per-artery analysis, subjects with LAD occlusion had more dysfunctional segments than segments showing HE (8.5 ± 3.1 vs. 7.7 ± 2.2, $p < 0.05$), whereas

Table 2. Positive Predictive Value of HE Presence According to the IRA

Segment Number	LAD	RCA	LCX
1. Basal anterior	95 (76–99)	—	5 (1–24)
2. Basal anteroseptal	100 (88–100)	—	—
3. Basal inferoseptal	7 (2–21)	83 (66–92)	10 (4–26)
4. Basal inferior	—	89 (74–95)	11 (5–26)
5. Basal inferolateral	—	23 (10–48)	76 (52–90)
6. Basal anterolateral	11 (2–44)	—	89 (55–97)
7. Mid-anterior	100 (91–100)	—	—
8. Mid-anteroseptal	100 (92–100)	—	—
9. Mid-inferoseptal	39 (26–53)	52 (38–66)	9 (4–21)
10. Mid-inferior	2 (0–12)	73 (58–84)	25 (15–39)
11. Mid-inferolateral	—	30 (15–52)	70 (48–85)
12. Mid-anterolateral	80 (58–92)	—	20 (8–42)
13. Apical anterior	100 (92–100)	—	—
14. Apical septal	86 (73–93)	14 (7–27)	—
15. Apical inferior	56 (42–69)	33 (22–47)	10 (5–22)
16. Apical lateral	70 (51–84)	—	30 (16–49)
17. Apex	91 (80–96)	4 (1–14)	2 (0–11)

Data expressed as percentages (95% confidence interval).
HE = hyperenhancement; IRA = infarct related artery; other abbreviations as in Table 1.

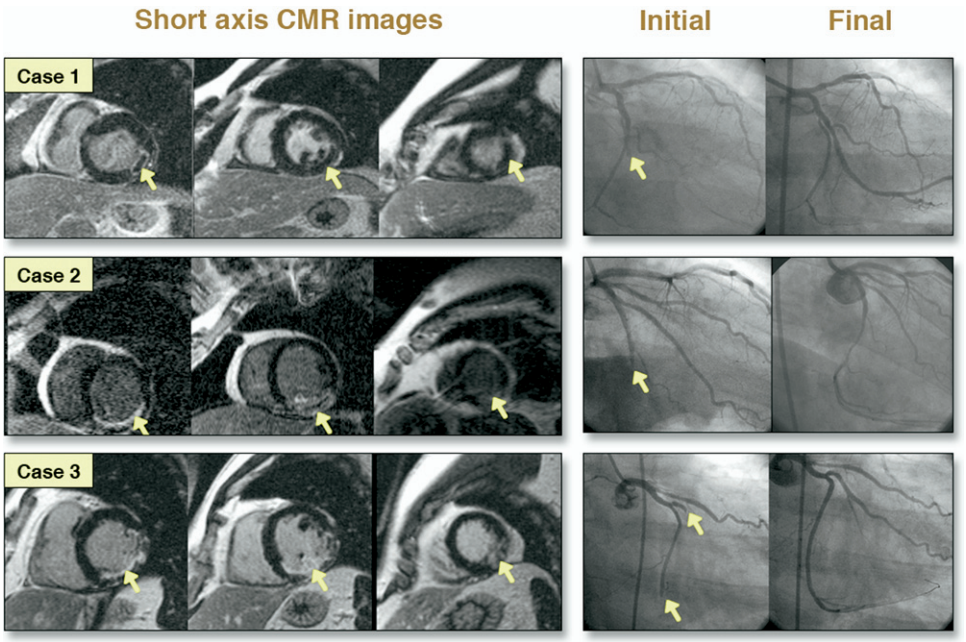

Figure 4. Distribution of HE Due to Occlusion of the LCX Artery

Three examples that illustrate the wide variability in HE location on CMR images **(left panels)** and the corresponding coronary anatomy by angiography before and after PCI **(right panels)**. **Yellow arrows** point out the site of the occlusion. Case 1 is a focal lateral infarction due to occlusion of a second well-developed obtuse marginal branch. Case 2 is an inferior infarction following occlusion of a distal codominant LCX artery. Case 3 is an occlusion of a large marginal branch and distal embolization of a dominant LCX artery. As a result, HE extends from the basal anterolateral wall to the basal inferoseptal territory. Abbreviations as in Figure 1.

patients with no anterior infarction did not (4.4 ± 2.0 vs. 4.2 ± 2.0, p = 0.3).

Association with ECG ST-segment elevation. The number of leads with ST-segment elevation averaged 3.8 ± 1.5. The total number of segments with HE (6.0 ± 2.6) loosely correlated with the number of ECG leads with ST-segment elevation (3.8 ± 1.5; R = 0.32, p = 0.002). A STEMI to the LAD typically had a high percentage of subjects with ST-segment elevation in leads I (93%), aVL (90%), V_1 (73%), V_2 (91%), V_3 (92%), and V_4 (76%). Similarly, RCA infarcts presented with ST-segment elevation in leads II (76%), III (74%), and aVF (80%). No lead was

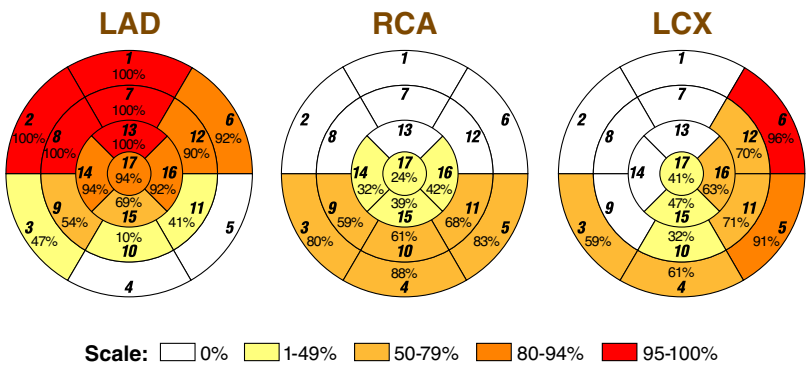

Figure 5. Specificity of Regional Dysfunction According to the IRA

Bulls-eye diagrams showing the extent and specificities of regional wall motion abnormalities according to the IRA. Five segments were 100% specific for LAD occlusion, but none was 100% specific for RCA or LCX occlusion. **Italicized numbers** designate the segment number. Abbreviations as in Figures 1 and 3.

Table 3. Percentage of Patients With HE Presenting With ST-Segment Elevation

	ECG Leads With ST-Segment Elevation >1 mV											
	I	aVL	II	III	aVF	aVR	V_1	V_2	V_3	V_4	V_5	V_6
1. Basal anterior	**60**	**55**	2	0	0	29	27	44	44	41	31	10
2. Basal anteroseptal	**60**	**55**	2	0	0	43	**58**	**60**	**62**	46	31	5
3. Basal inferoseptal	13	10	**67**	2	**65**	29	12	5	8	19	27	48
4. Basal inferior	0	0	**74**	**79**	**78**	29	15	2	3	19	31	**57**
5. Basal inferolateral	7	10	24	28	23	29	4	2	5	14	27	43
6. Basal anterolateral	13	15	5	5	3	14	8	7	5	11	15	14
7. Mid-anterior	**93**	**90**	5	2	3	43	**62**	**81**	**82**	**70**	46	19
8. Mid-anteroseptal	**87**	**85**	5	2	3	**57**	**77**	**91**	**92**	**73**	46	19
9. Mid-inferoseptal	**53**	40	**62**	**58**	**60**	0	31	42	46	**59**	**62**	**67**
10. Mid-inferior	13	15	**81**	**84**	**83**	43	23	9	8	**27**	**42**	**62**
11. Mid-inferolateral	7	10	29	33	28	29	8	5	5	16	31	48
12. Mid-anterolateral	**60**	**65**	2	2	3	29	19	37	36	35	31	14
13. Apical anterior	**93**	**90**	7	5	5	43	**73**	**91**	**92**	**76**	**50**	19
14. Apical septal	**87**	**85**	24	21	23	43	**73**	**86**	**90**	**76**	**50**	29
15. Apical inferior	**73**	**60**	48	47	48	14	42	**60**	**67**	**70**	**65**	**52**
16. Apical lateral	**60**	**65**	10	9	5	29	31	40	38	46	46	38
17. Apex	**93**	**90**	14	9	13	43	**69**	**86**	**87**	**78**	**58**	29

Data expressed as the number of patients with HE in a particular segment as a percentage of the total number of ECGs with ST-segment elevation in a particular lead. **Bold** values indicate percentages ≥50%.
ECG = electrocardiogram; other abbreviations as in Table 2.

associated with a high percentage for LCX infarcts. The percentage of subjects presenting with ST-segment elevation with corresponding HE is shown in Table 3.

Agreement between HE location and the AHA 17-segment model. Figure 6 illustrates the agreement between the observed HE distribution and the coronary arterial supply. In a per-segment analysis, 132 (23.4%) out of 564 segments with HE were found to differ from the coronary distribution empirically assigned with the 17-segment model. According to the IRA, 12 (4.4%) of 270 LAD segments with HE, 46 (49.5%) of 93 LCX segments, and 74 (36.8%) of 127 segments for the RCA were found to be discordant. The agreement was remarkably low for the mid-anterolateral (segment 12) and apical lateral (segment 16) segments, 20% and 29.6%, respectively. These segments are empirically attributed to the LCX, but for all these segments, the culprit lesion was located in the LAD, with the exception of 1 ramus occlusion. The agreement was also low in the apical inferior (segment 15), attributed to the RCA, which was 66.6% of the time related to an LAD or LCX occlusion.

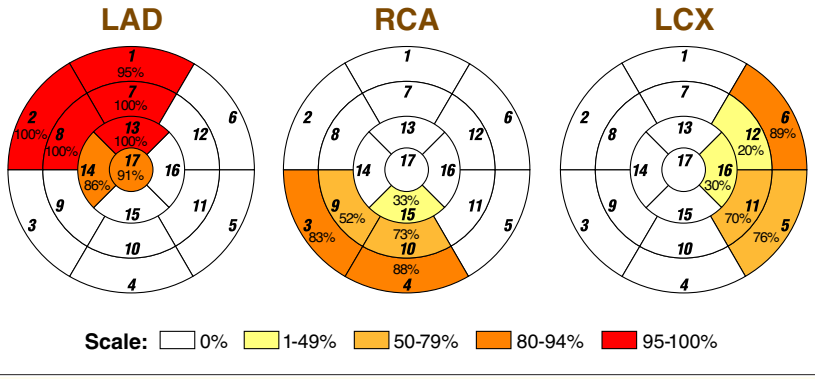

Figure 6. Percentage Agreement of Observed HE Within Each IRA Zone as Proposed by the AHA Segmentation

Bulls-eye diagrams illustrating the agreement of the observed CMR HE confined to each American Heart Association (AHA)-proposed coronary arterial distribution. Percent numbers equate to the percentage of times that HE was appropriately assigned to the empirical coronary artery distribution proposed by the AHA. **Italicized numbers** designate the segment number. Abbreviations as in Figures 1 and 3.

In a per-patient analysis, perfect agreement between the observed HE on CMR and the 17-segment model was found in only 33% of patients (18.0% for the LAD, 21.4% for the LCX, and 55.9% for the RCA occlusion, respectively). The mean number of discordant segments per patient was 1.4 ± 1.4 (1.9 ± 1.3 for LAD, 2.7 ± 1.8 for the LCX, and 0.6 ± 0.8 for the RCA occlusion).

DISCUSSION

The primary goal of this study was to assess the correspondence between the coronary arteries distribution and the supplied myocardium according to the 17-segment model. We studied this relationship in a cohort of patients admitted with their first STEMI who had an occluded artery at the time of primary PCI. Using this methodology and CMR imaging, we were able to show that only 4 segments were completely specific for LAD occlusion and none was specific for RCA or LCX occlusion. These results emphasize the tremendous individual variability of coronary artery distribution, which is much greater than that empirically assigned to the 17-segment model segmentation. Additionally, our data suggest that the apical inferior and apical inferolateral segments should be considered part of the LAD territory rather than the RCA and LCX territories as previously recommended (Fig. 7).

The results of nuclear scintigraphy have previously been used to establish the foundation between coronary angiography and the location of supplied myocardium (2). Technetium-99m compounds are perfusion agents that accumulate in the myocardium in proportion to myocardial blood flow and undergo minimal redistribution. The myocardial area supplied by a particular coronary artery can therefore be established during percutaneous coronary angioplasty occlusion (2,8,9). Following prolonged ischemic injury, the subendocardial region rapidly becomes necrotic and establishes a circumferential extent of necrosis. Our group previously demonstrated this "wave-front" phenomenon in patients using CMR imaging. Therefore, in a group of patients following STEMI, the extent of myocardial HE would accurately portray this same myocardial risk area subtended by the IRA (6). Additionally, CMR imaging can identify important myocardial landmarks—such as papillary muscles or the interventricular grooves—to couple with the anatomical course of the coronary arteries and to better aid in correlating the myocardial segmentation with coronary angiography. No previous study had used this hypothesis of myocardial infarction to systematically assign each of the 17 LV segments to each of the 3 major coronary arteries.

Although significant individual variability was assumed in the original report from the AHA, each of the 17 segments was believed to be appropriately assigned to 1 of the major coronary arteries based on existing data in 35 patients (2). Our findings provide additional objective evidence regarding the assignment of coronary arterial perfusion territories in a larger cohort of patients using a high-resolution modality capable of directly visualizing myocardial infarction. However, the results of this study further highlight that in a per-segment analysis, only 76% of segments followed the distribution of coronary arteries empirically attributed and discordance reached 67% of cases in a per-patient analysis. In contrast to the AHA report that attributed the greatest variability in coronary artery distribution to the apical segment (segment 17), our data suggest the greatest variability occurs at the apical lateral wall (segment 16), which can be supplied by any of the 3 coronary arteries. The greatest disagreement occurred in the mid-anterolateral (segment 12) and apical lateral (segment 16) wall, originally assigned to the LCX artery and inferoapical segment originally attributed to the RCA. As seen in Figure 7, the entire apex is more appropriately assigned to the territory of the LAD. Extending the coverage of the LAD in our 17-segment model more accurately portrays the large amount of myocardium supplied by this artery and provides an anatomical basis for the large infarct size and high potential

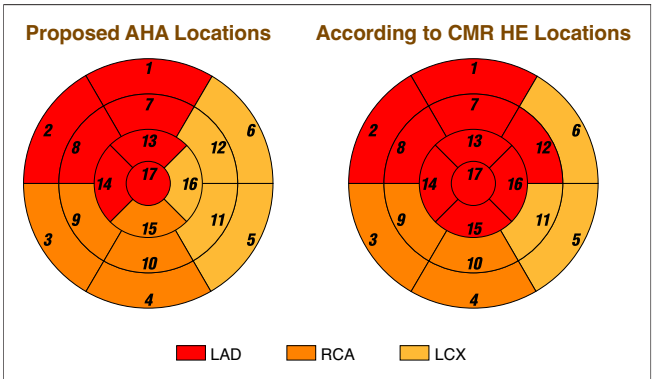

Figure 7. Segmentation of Coronary Arterial Distribution

Segmentation of coronary arterial distribution within the 17-segment model as proposed by the AHA **(left bulls-eye diagram)** and as according to the maximum specificity of CMR HE **(right bulls eye diagram)**. Results of this study suggest that the LAD territory in most cases supply additional segments in the apex (segments 15 and 16) and the mid-anterolateral wall (segment 12). **Italicized numbers** designate the segment number. Abbreviations as in Figures 1 and 6.

for adverse ventricular remodeling associated with LAD infarctions.

The correspondence between the coronary artery anatomy and the 17-segment model was also recently reported by Pereztol-Valdés et al. (9) using nuclear perfusion in a cohort of patients with single vessel disease population referred for elective PCI. Consistent with that previous report, our study also shows that the greatest overlap in coronary artery distribution occurs in the inferolateral region corresponding either to RCA or LCX territories, as well as the inferoseptal region that may be supplied by the LAD artery, RCA, or even a left-dominant LCX artery. However, there are some differences between the 2 studies that are worthy of mention. In our CMR study, only 4 segments (segments 2, 7, 8, and 13) were found to be 100% specific for LAD occlusion as opposed to 8 segments (segments 1, 2, 7, 8, 13, 14, 16, and 17) reported by Pereztol-Valdés. One patient with a proximal ramus occlusion had HE located in the basal anterior segment (segment 1), 7 subjects with RCA occlusion had HE in the apical septum (segment 14), and up to 8 subjects with LCX occlusion developed HE in the apical lateral wall (segment 16). We also found HE involving the apex (segment 17) in the setting of RCA and LCX occlusion. Several reasons might have accounted for these differences. First, these disparities may be simply explained because of the increased number of subjects included in our study, leading to increased variability in coronary arterial anatomy and dominance. Second, the increased spatial resolution of delayed enhanced CMR and the absence of attenuation artifacts as compared with nuclear perfusion techniques may contribute to the increased detection of segments with subendocardial infarction in the periphery of the area at risk, that otherwise could have been missed by single photon emission computed tomography. Third, CMR imaging can identify the interventricular grooves for better coronary angiography registration. Finally, nuclear perfusion imaging looks at ischemia, whereas contrast-enhanced CMR identifies necrosis or fibrosis. Infarct appears as long as ischemia persists, a process that is influenced by the time of coronary occlusion and the presence of collateral flow. In this regard, we have confirmed a trend to a higher degree of collateral flow among subjects presenting with RCA occlusion. This trend might have resulted in a smaller extent of HE in such cases and, consequently, a reduction in the amount of myocardium allocated to the RCA. Discrimination between RCA and LCX involvement based solely on the involvement of individual myocardial segments is difficult. Concomitant observation of the anterolateral, lateral, and inferior walls may assist the evaluation. In our study, analysis of adjacent segments helped to clarify the localization of disease. Thus, any combination of HE in the anterolateral wall and inferior wall was completely specific for a left dominant or codominant occlusion. Presence of HE in the inferolateral wall (segments 5 and 11) with or without HE in the anterolateral segments was highly specific of a nondominant LCX occlusion as well.

Detection of multivessel disease is of crucial importance in the management of coronary artery disease. Multiple studies have demonstrated improved outcomes and prognosis by reperfusion with bypass surgery or PCI in this situation (10–12). Functional imaging techniques must therefore provide precise knowledge of coronary artery distribution to allow appropriate identification of multivessel disease. This capability has been extensively studied in nuclear perfusion imaging experimentally (13,14) and clinically, using several methodologies in patients with acute myocardial infarction (15) and elective PCI (16–19). Several attempts for fusing anatomic images from the coronary arteries and functional information from different modalities have been proposed in an effort to assist in locating and assessing the physiologic significance of multiple stenotic lesions. Faber et al. (20) proposed an algorithm based on the integration of nuclear perfusion imaging with conventional coronary angiography. The CMR is now widely used for function, perfusion, and viability assessment. Because of the paucity of studies correlating CMR imaging with coronary anatomy, most decisions concerning the involvement of coronary arteries when interpreting CMR viability and perfusion imaging studies are extrapolated from previous work based on nuclear perfusion techniques. Setser et al. (21) studied the correspondence between the myocardial 17-segment model and coronary anatomy by coupling information from CMR images and noninvasive computed tomography coronary angiography in a small series of 26 patients. In line with our findings, the authors showed that the maximal discordance of coronary distribution occurred in the mid-anterolateral, apical lateral, and apical inferior wall (segments 12, 15, and 16), which were supplied by the LAD in most cases. They also found that the combined information provided by fusion of images was useful for the planning of surgery in those patients. However,

fusion of different modalities may be subject to misregistration or misalignment. Thus new technologies capable of obtaining both coronary anatomy and functional information in a single study—such as positron emission tomography/computed tomography scanners or coronary MR angiography/functional CMR—would be better suited for this purpose.

Study limitations. This study includes research subjects participating in a prospective observational study investigating the impact of microvascular perfusion and infarct size on LV remodeling. No investigational treatments were performed, but participation in this study was voluntary and may not totally reflect findings for all patients following acute myocardial infarction.

Additionally, the allocation of the IRA territory might be underestimated in patients who develop congestive heart failure during hospital admission, because this clinical situation is a contraindication for a CMR study. Almost two-thirds of the patients had multivessel disease. It is unlikely, however, that significant coronary disease in vessels other than the IRA could have affected the extent and location of HE. In this regard, 8 patients with an additional area of remote HE clearly not corresponding to the IRA territory showed an occlusion in a coronary artery different than the IRA were excluded. Additionally, we studied a population following an acute STEMI, and the results of this study may vary in the setting of chronic coronary artery disease, where well-developed collaterals might reduce the extent of infarction.

CONCLUSIONS

In patients presenting with STEMI, direct visualization of infarcted myocardium and anatomical landmarks by high-resolution CMR imaging, enables registration between affected myocardial segments and the occluded artery by invasive angiography. The results of our findings bring objective evidence to the assignment of coronary arterial perfusion territories within the 17-segment model. Only 4 segments were completely specific for LAD occlusion, and no single segment could be exclusively attributed to a RCA or LCX occlusion. However, analysis of adjacent segments increased the specificity for a given coronary occlusion. The LAD territory is larger than the AHA-proposed 17-segment model and is most often responsible for myocardial infarctions involving the mid-anterolateral and all apical segments. These findings will aid in the appropriate assignment of the culprit vessel in CMR studies and may also influence the interpretation of other noninvasive modalities.

Reprint requests and correspondence: Dr. Edwin Wu, 201 E Huron, Galter 10-240, Chicago, Illinois 60611. *E-mail: ed-wu@northwestern.edu.*

REFERENCES

1. Cerqueira MD, Weissman NJ, Dilsizian V, et al. Standardized myocardial segmentation and nomenclature for tomographic imaging of the heart: a statement for healthcare professionals from the Cardiac Imaging Committee of the Council on Clinical Cardiology of the American Heart Association. Circulation 2002;105:539–42.
2. Gallik DM, Obermueller SD, Swarna US, Guidry GW, Mahmarian JJ, Verani MS. Simultaneous assessment of myocardial perfusion and left ventricular function during transient coronary occlusion. J Am Coll Cardiol 1995;25:1529–38.
3. Plein S, Ridgway JP, Jones TR, Bloomer TN, Sivananthan MU. Coronary artery disease: assessment with a comprehensive MR imaging protocol—initial results. Radiology 2002;225:300–7.
4. Misko J, Dziuk M, Skrobowska E, Szalus N, Pietrzykowski J, Warczynska A. Co-registration of cardiac MRI and rest gated SPECT in the assessment of myocardial perfusion, function and viability. J Cardiovasc Magn Reson 2006;8:389–97.
5. Wagner A, Mahrholdt H, Holly TA, et al. Contrast-enhanced MRI and routine single photon emission computed tomography (SPECT) perfusion imaging for detection of subendocardial myocardial infarcts: an imaging study. Lancet 2003;361:374–9.
6. Ortiz-Perez JT, Meyers SN, Lee DC, et al. Angiographic estimates of myocardium at risk during acute myocardial infarction: validation study using cardiac magnetic resonance imaging. Eur Heart J 2007;28:1750–8.
7. Simonetti OP, Kim RJ, Fieno DS, et al. An improved MR imaging technique for the visualization of myocardial infarction. Radiology 2001;218:215–23.
8. Fram DB, Azar RR, Ahlberg AW, et al. Duration of abnormal SPECT myocardial perfusion imaging following resolution of acute ischemia: an angioplasty model. J Am Coll Cardiol 2003;41:452–9.
9. Pereztol-Valdés O, Candell-Riera J, Santana-Boado C, et al. Correspondence between left ventricular 17 myocardial segments and coronary arteries. Eur Heart J 2005;26:2637–43.
10. Hamm CW, Reimers J, Ischinger T, Rupprecht HJ, Berger J, Bleifeld W. A randomized study of coronary angioplasty compared with bypass surgery in patients with symptomatic multivessel coronary disease. German Angioplasty Bypass Surgery Investigation (GABI). N Engl J Med 1994;331:1037–43.
11. Hannan EL, Racz MJ, Walford G, et al. Long-term outcomes of coronary-artery bypass grafting versus stent implantation. N Engl J Med 2005;352:2174–83.
12. The final 10-year follow-up results from the BARI randomized trial. J Am Coll Cardiol 2007;49:1600–6.

13. De Coster PM, Wijns W, Cauwe F, Robert A, Beckers C, Melin JA. Area-at-risk determination by technetium-99m-hexakis-2-methoxyisobutyl isonitrile in experimental reperfused myocardial infarction. Circulation 1990;82:2152–62.
14. Sinusas AJ, Trautman KA, Bergin JD, et al. Quantification of area at risk during coronary occlusion and degree of myocardial salvage after reperfusion with technetium-99m methoxyisobutyl isonitrile. Circulation 1990;82:1424–37.
15. Gibbons RJ, Verani MS, Behrenbeck T, et al. Feasibility of tomographic 99mTc-hexakis-2-methoxy-2-methylpropyl-isonitrile imaging for the assessment of myocardial area at risk and the effect of treatment in acute myocardial infarction. Circulation 1989;80:1277–86.
16. Borges-Neto S, Puma J, Jones RH, et al. Myocardial perfusion and ventricular function measurements during total coronary artery occlusion in humans. A comparison with rest and exercise radionuclide studies. Circulation 1994;89:278–84.
17. Borges-Neto S, Watson JE, Miller MJ. Tc-99m sestamibi cardiac SPECT imaging during coronary artery occlusion in humans: comparison with dipyridamole stress studies. Radiology 1996;198:751–4.
18. Ceriani L, Verna E, Giovanella L, Bianchi L, Roncari G, Tarolo GL. Assessment of myocardial area at risk by technetium-99m sestamibi during coronary artery occlusion: comparison between three tomographic methods of quantification. Eur J Nucl Med 1996;23:31–9.
19. Pereztol-Valdés O, Candell-Riera J, Oller-Martinez G, et al. [Localization and quantification of myocardium at risk by myocardial perfusion SPECT during coronary artery occlusion]. Rev Esp Cardiol 2004;57:635–43.
20. Faber TL, Santana CA, Garcia EV, et al. Three-dimensional fusion of coronary arteries with myocardial perfusion distributions: clinical validation. J Nucl Med 2004;45:745–53.
21. Setser RM, O'Donnell TP, Smedira NG, et al. Coregistered MR imaging myocardial viability maps and multidetector row CT coronary angiography displays for surgical revascularization planning: initial experience. Radiology 2005;237:465–73.